Journal of Molecular Catalysis A: Chemical 309 (2009) 146–152

Contents lists available at ScienceDirect

Journal of Molecular Catalysis A: Chemical

journal homepage: www.elsevier.com/locate/molcata

Bimetallic mesoporous materials for high yield synthesis of carbon nanotubes by chemical vapour deposition techniques

R. Atchudan [a], A. Pandurangan [a,b,*], T. Somanathan [a]

[a] Department of Chemistry, Center for Nanoscience & Technology, Anna University, CEG, Sardhar Patel Road, Guindy, Chennai, Tamil Nadu 25, India
[b] Institute of Catalysis & Petroleum Technology, Anna University, Chennai 25, India

ARTICLE INFO

Article history:
Received 24 June 2008
Received in revised form 6 February 2009
Accepted 13 May 2009
Available online 22 May 2009

Keywords:
SWNT
CVD
Acetylene
Fe–Zn-MCM-41

ABSTRACT

Mesoporous Fe-MCM-41, Zn-MCM-41 and Fe–Zn-MCM-41 molecular sieves were synthesized in various Si/metal ratios by the hydrothermal method. The synthesized materials were characterized by various physicochemical techniques such as XRD, N_2 adsorption–desorption isotherm, TGA, DRS-UV spectroscopy, SEM and TEM. The catalytic activity of monometallic Fe-MCM-41, Zn-MCM-41 and bimetallic Fe–Zn-MCM-41 molecular sieves was tested and optimized for the maximum yield of carbon nanotubes (CNTs) by decomposition of acetylene (C_2H_2) at 700–900 °C. The deposited carbon materials were purified and characterized by XRD, SEM, TEM and Raman spectroscopy techniques. The purified samples show the presence of well-graphitized SWNTs over the bimetallic Fe–Zn-MCM-41 (3:1) molecular sieve. It was found that Fe–Zn-MCM-41 in the ratio of 3:1 (Fe:Zn) contains an optimum amount of metal to form metallic clusters, which in turn leads to the formation of CNTs with higher carbon deposition. The diameters of the carbon nanotubes are in the range of 1.2–2.5 nm, which was revealed by the Raman spectroscopy. This study shows that the bimetallic Fe–Zn-MCM-41 mesoporous molecular sieve as a promising catalytic template with good thermal stability and high productivity for the synthesis of CNTs.

1. Introduction

Iijima's discovery of a quasi one-dimensional new type of carbon named the "carbon nanotube" (CNT) [1,2] attracted a great deal of attention in various fields of research, due to its superior mechanical strength [3], electronic properties [4], large surface area for adsorption of hydrogen [5] and high aspect ratio. Generally, CNTs are synthesized by three different techniques: (i) arc discharge between two graphite electrodes [6]; (ii) laser evaporation of carbon target [7]; and (iii) chemical vapour deposition (CVD) through catalytic decomposition of hydrocarbons [8]. The first two methods employ the solid-state carbon precursors needed for carbon evaporation at high temperature. The CVD utilizes hydrocarbon gases as carbon sources and metal nanoparticles as the seeds for CNT growth. The CVD method has several advantages which include purity, high yield, selective growth and vertical alignment. The catalytically produced tubes are adequate for many applications, especially because they can be directly synthesized without major contamination by carbonaceous impurities. Various catalytic chemical vapour deposition (CCVD) methods are already known for the production of single-walled carbon nanotubes (SWNTs) using different carbon precursors [9–11]. Among the carbon sources utilized for SWNT production, CCVD studies with acetylene are limited due to the following reasons [12–14]. Acetylene is considered as a good carbon source for SWNTs production because it contains fewer number of carbon atoms per molecule and greater activity in comparison to other hydrocarbons such as benzene [15].

Generally, zeolite pores are limited to micropores (diameter <1.3 nm) and the channel size cannot be varied without synthesizing materials that have a different structure and composition. Thus zeolites are not an ideal choice for the synthesis of SWNTs because of their lack of pore size flexibility. Hence, the above drawbacks can be overcome by the introduction of mesoporous molecular sieves. In 1992, researchers at Mobil Research and Development Corporation reported the synthesis of a new family of mesoporous molecular sieves (M41S) with exceptionally large uniform pore structures [16,17]. Transition metal catalysts can be incorporated into the pore walls of the mesoporous molecular sieves that stabilize dispersed catalytic sites and also exhibit good structural stability. The M41S family comprising MCM-41 and related mesoporous molecular sieves are of interest because of their remarkable properties such as large surface area (>1000 m^2/g), pore volume (>0.8 cm^3/g), narrow pore size distribution, and the ease with which their surface can be functionalized [17]. Their uniform and tunable pore diameters make them also well adapted for good catalytic supports. Generally, pure siliceous MCM-41 has limited catalytic activity, but active catalytic sites can be generated in Si-MCM-41 by isomorphously substituting silicon with transition metals [18]. Sev-

* Corresponding author. Tel.: +91 44 22203518; fax: +91 44 22352642.
E-mail address: pandurangan_a@yahoo.com (A. Pandurangan).

1381-1169/$ – see front matter © 2009 Elsevier B.V. All rights reserved.
doi:10.1016/j.molcata.2009.05.010

eral studies have been dedicated to the investigation of transition metal substituted MCM-41 because of their wide range of applications in catalysis [19–21]. The metal particle plays an important role during CNT production and reports showing a direct correlation between the size of the metal nanoparticles and the eventual tube diameter [22].

In the growth of CNTs, dispersion of metal particles over the support plays an important role in the formation of well-graphitized CNTs. In the present work, we have synthesized Fe-MCM-41, Zn-MCM-41and Fe–Zn-MCM-41 as catalytic templates for the growth of CNTs by the CVD method using acetylene as carbon precursor. The maximum yield of CNTs was found in bimetallic Fe–Zn-MCM-41 than in monometallic Fe-MCM-41 and Zn-MCM-41. The diameters of the well-graphitized CNTs are in the range of 1.2–2.5 nm formed over the pores of MCM-41 mesoporous materials are clearly observed by Raman spectroscopy. The purified CNTs were characterized by XRD, SEM, TEM and Raman spectroscopy. The ultimate goal of this study is to understand the correlation between the Fe-MCM-41, Zn-MCM-41 and Fe–Zn-MCM-41 catalytic templates and the quantity of the carbon nanotubes produced.

2. Experimental

2.1. Materials

The chemicals used for the synthesis of mesoporous molecular sieves were sodium metasilicate (Qualigens), zinc acetate (Merck) and ferric nitrate (Merck) as sources of silicon, zinc and iron, respectively. Cetyltrimethylammonium bromide (CTAB) (Merck) was used as the structure-directing agent. Sulphuric acid (Merck) was used to adjust the pH of the medium.

2.2. Synthesis of metal-incorporated MCM-41 molecular sieves

Fe-MCM-41 (Si/Fe = 100), Zn-MCM-41 (Si/Zn = 100) and Fe–Zn-MCM-41 (Si/Fe + Zn = 100) (Fe:Zn ratios: 1:4, 1:3, 1:2, 1:1, 2:1, 3:1 and 4:1) were synthesized by the direct hydrothermal method. The gel composition of SiO_2: xM:0.2CTAB:0.89H_2SO_4:120H_2O (where M = metal and x = various ratios of metal) was prepared. In a typical synthesis procedure, sodium metasilicate in water was combined with an appropriate amount of metal salts in distilled water and the pH of the solution was adjusted to 10.5 by adding 4N H_2SO_4 with constant stirring to form a gel. After 30 min, an aqueous solution of CTAB was added to it and the mixture was stirred for 1 h at room temperature. The suspension was then transferred into a 300 ml stainless steel autoclave, sealed and heated in a hot air oven at 145 °C for 48 h. After crystallization, Fe, Zn and Fe–Zn-MCM-41 materials were recovered by filtration, washed with double distilled water and dried at 100 °C for 5 h. The final active catalyst was obtained by removing the occluded surfactant by calcining the sample at 550 °C in air for 5 h.

2.3. Synthesis of carbon nanotubes

The catalytic reaction for the synthesis of CNTs was carried out using the above synthesized Fe, Zn and Fe–Zn-MCM-41. The experiments on the production of CNTs were carried out in a simple CVD setup containing horizontal tubular furnace and gas flow control units. In a typical growth experiment, ca. 100 mg catalyst was placed in a quartz boat inside a quartz tube. The catalyst was purged in a nitrogen stream at a flow rate of 100 ml/min for 10 min in order to remove water and pre-treat the catalyst. The reaction was carried out using acetylene as carbon source at 700–900 °C at a flow rate of 60 ml/min for 10 min. The furnace was then cooled to room temperature under nitrogen atmosphere and the final product formed was a black material after the completion of the reaction. The material was then weighed, purified and characterized. The percentage of carbon deposited due to the catalytic decomposition of acetylene was obtained from the following equation:

$$\text{carbon deposit}\,(\%) = \frac{m_{\text{tot}} - m_{\text{cat}}}{m_{\text{cat}}} \times 100$$

where m_{cat} and m_{tot} are the mass of the catalyst before and after the reaction, respectively.

2.4. Purification of synthesized carbon nanotubes

The removal of the silica phase was carried out by treating the carbon deposited material with 40% hydrofluoric acid (HF) at ambient temperature as reported in earlier literature [23,24]. About 200 mg of as-synthesized carbon sample was mixed with appropriate amount of HF. The obtained sample was further treated with hydrochloric acid to remove the metal particles and washed with double distilled water and then with acetone. The filtered material was dried at 100 °C for 5 h in air atmosphere [25].

2.5. Characterization methods

The synthesized metal-incorporated mesoporous MCM-41 materials and CNTs were characterized by various physico-chemical techniques such as XRD, N_2 adsorption–desorption isotherm, TGA–DTA, DRS-UV, SEM, TEM and Raman spectroscopy. The X-ray powder diffractograms of calcined catalysts and purified CNT samples were obtained on a Philips PW 1050 diffractometer equipped with a liquid nitrogen cooled germanium solid-state detector using Cu Kα radiation. The diffractogram of metal-incorporated MCM-41 and CNTs were recorded in the 2θ range of 1–10° and 5–80°, respectively, and at the scanning rate of 0.02° with the counting time of 5 s at each point. N_2 adsorption–desorption isotherms were measured at −197 °C using a Micromeritics ASAP 2000. Prior to the experiments, the samples were dried at 130 °C and evacuated overnight for 8 h in flowing argon at a flow rate of 60 ml/min at 200 °C. Surface area, pore size and pore volumes were obtained from these isotherms using the conventional BET and BJH equations. Thermogravimetric and differential thermal analysis was performed using a Shimadzu DTG 60 Thermal Analyzer. Samples of approximately 10 mg were heated in air from 25 to 1000 °C, at heating rate of 10 °C/min. DRS-UV analysis was performed using a Shimadzu UV-2450 model and a $BaSO_4$ white plate used as a reference. SEM images were obtained on a JEOL JSM 840A electron microscope with beam energy of 4 kV by placing the calcined MCM-41 and as-grown CNT materials on conductive carbon tape. The TEM images of mesoporous MCM-41 and CNTs were obtained using a JEOL JEM-2000 FX 11 electron microscope operated at 300 kV. Samples for TEM were prepared by placing droplets of a suspension of the sample in acetone on a polymer microgrid supported on a Cu grid. Raman spectra were recorded with a Micro-Raman system RM 1000 Renishaw using a laser excitation line at 532 nm (Nd-YAG), 0.5–1 mW, with 1 μm focus spot in order to avoid photodecomposition of the samples.

3. Results and discussion

3.1. Characterizations of synthesized mesoporous MCM-41 catalysts

3.1.1. X-ray diffraction pattern of catalysts

The small-angle powder XRD patterns of Fe, Zn and Fe–Zn-MCM-41 samples are shown in Fig. 1(a–c). X-ray diffraction techniques are useful for the characterization of M41S group materials. The calcined MCM-41 material shows a strong peak between 1.8° and 2.8°

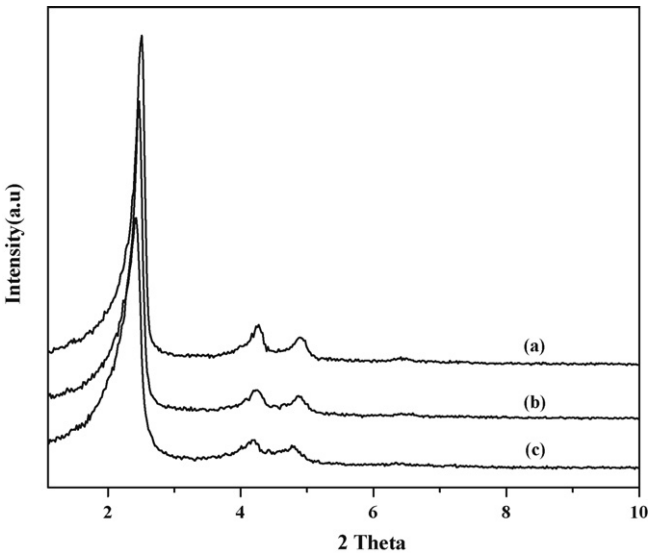

Fig. 1. X-ray diffraction pattern of mesoporous molecular sieves: (a) Fe-MCM-41 (100), (b) Fe–Zn-MCM-41 (100) and (c) Zn-MCM-41 (100).

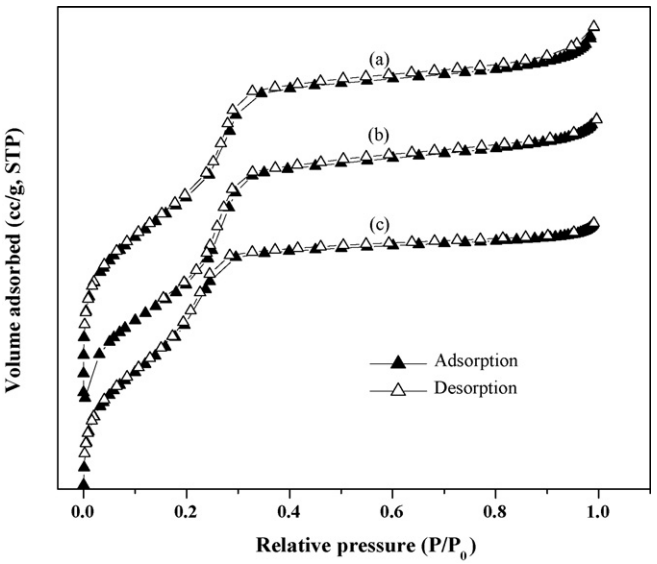

Fig. 2. Nitrogen adsorption–desorption isotherms of (a) Fe-MCM-41 (100), (b) Fe–Zn-MCM-41 (100) and (c) Zn-MCM-41 (100).

(2θ), due to (1 0 0) diffractions lines and weak peaks between 3.8° and 4.8° (2θ), and 6.2° and 6.7° (2θ) due to higher order (1 1 0), (2 0 0) and (2 1 0) diffractions indicating the formation of well-ordered mesoporous materials. All these patterns are assigned to hexagonal symmetry [17]. XRD patterns of the calcined material prove that there is neither collapse of the structure nor change of the phase during calcination. This suggests that the MCM-41 material has high thermal stability after calcination as well supported by Chen et al. [26].

3.1.2. Nitrogen adsorption–desorption isotherms

BET surface area, pore size and pore volume of calcined Fe-MCM-41, Zn-MCM-41 and Fe–Zn-MCM-41 materials are presented in Table 1. Adsorption and desorption isotherms for calcined Fe, Zn and Fe–Zn-MCM-41 materials are shown in Fig. 2. There are three distinct well-defined stages in the isotherm. The initial increase in the nitrogen uptake at low P/P_0 may be due to monolayer adsorption on the pore walls, a sharp step at intermediate P/P_0 may indicate the capillary condensation in the mesopores and a plateau portion at high P/P_0 associated with multilayer adsorption on the external surface of the catalysts. All the catalysts show a characteristic step around $P/P_0 \approx 0.3$ indicating the mesoporous nature of the materials [27]. The sharpness and height of the capillary condensation step are the indications of pore size uniformity. This step become gentler and was shifted to lower relative pressure with the increase in the metal content, which suggests that the pore size was narrowed and distributed. The specific surface area of samples determined by the BET surface area lies in the range of 923–978 m^2/g for Zn-MCM-41, Fe–Zn-MCM-41 and Fe-MCM-41. As shown in Table 1, the surface area, pore size and pore volume were higher for Fe-MCM-41 and Fe–Zn-MCM-41 than for Zn-MCM-41.

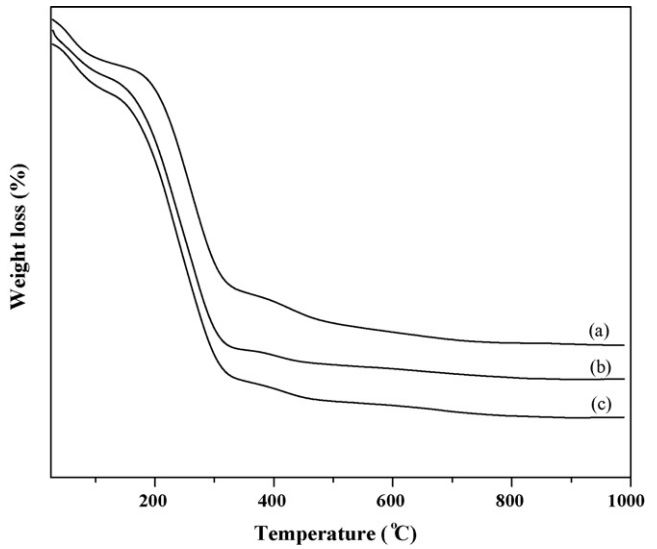

Fig. 3. Thermo gravimetric analysis of (a) Fe-MCM-41 (100), (b) Fe–Zn-MCM-41 (100) and (c) Zn-MCM-41 (100).

3.1.3. Thermogravimetric analysis of catalysts

The thermal properties of the samples were investigated by thermogravimetric analysis. The TGA and DTA profiles Fe-MCM-41, Fe–Zn-MCM-41 and Zn-MCM-41 are shown in Figs. 3 and 4, respectively. The thermogram of the materials shows three distinct weight losses. The initial weight loss up to 120 °C is due to desorption of physically adsorbed water. The weight loss from 120 to 350 °C is due to removal of organic template and the minute quantity of weight loss above 350–550 °C is related to water loss from

Table 1
Textural properties of the catalysts.

Catalyst	*d*-Spacing (nm)[a]	Surface area[b] (m^2/g)	Pore size[b] BJH_{ads} (nm)	Pore volume[b] BJH_{ads} (cc/g)
Fe-MCM-41 (100)	3.513	978	*2.538*	0.945
Fe–Zn-MCM-41 (100)	3.568	950	*2.501*	0.941
Zn-MCM-41 (100)	3.616	923	2.495	0.940

[a] The results obtained from XRD analysis.
[b] The values obtained from N_2 adsorption–desorption studies.

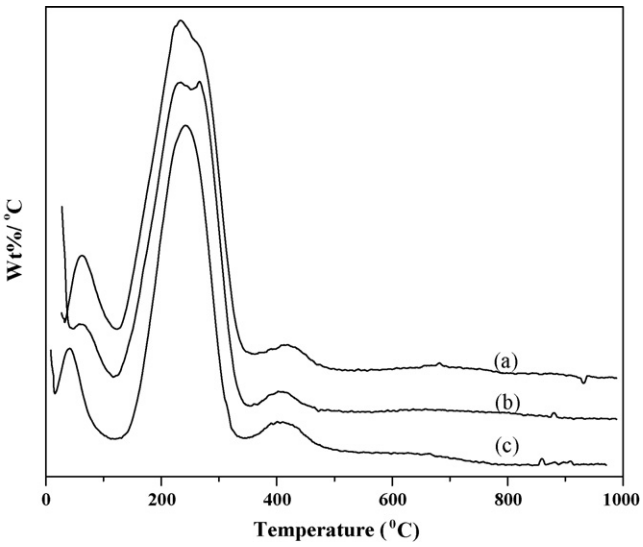

Fig. 4. DTA curves of (a) Fe-MCM-41 (100), (b) Fe–Zn-MCM-41 (100) and (c) Zn-MCM-41 (100).

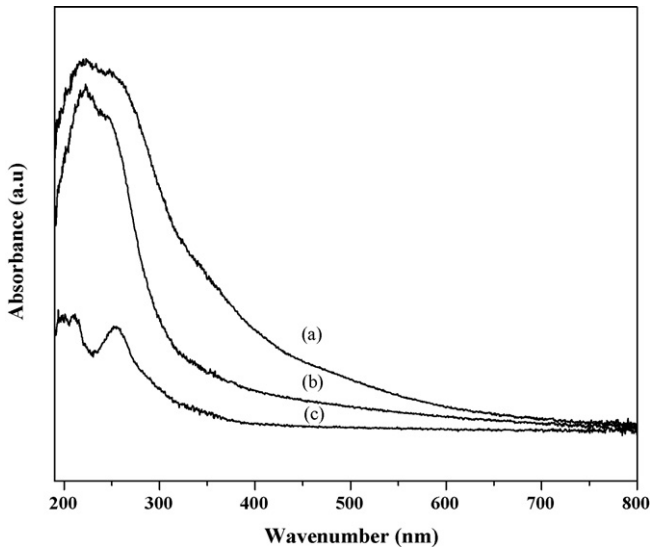

Fig. 5. DRS-UV spectra of (a) Fe–Zn-MCM-41 (100), (b) Fe-MCM-41 (100) and (c) Zn-MCM-41 (100).

the condensation of adjacent Si–OH groups to form siloxane bonds [28].

3.1.4. DRS-UV measurements of catalysts

The diffuse reflectance UV–visible spectra was recorded for the calcined Fe–Zn-MCM-41, Fe-MCM-41 and Zn-MCM-41 catalysts in order to study the co-ordination environment of Fe–Zn, Fe, Zn and their spectra are shown in Fig. 5(a–c), respectively. The appearance of the prominent absorption band at ca. 230 nm corresponds to the charge-transfer (CT) transitions of Fe(III) in $(FeO_4)^-$ tetrahedral geometry [29]. Zn-MCM-41 shows a prominent absorption band at ca. 256 nm corresponding to the CT transitions of Zn(IV) ions present in tetrahedral geometry.

3.1.5. SEM and TEM images of catalyst

The SEM and TEM images of the Fe-MCM-41, Fe–Zn-MCM-41 and Zn-MCM-41 samples are presented in Figs. 6 and 7. The SEM images show surface morphology and spongy like porous nature

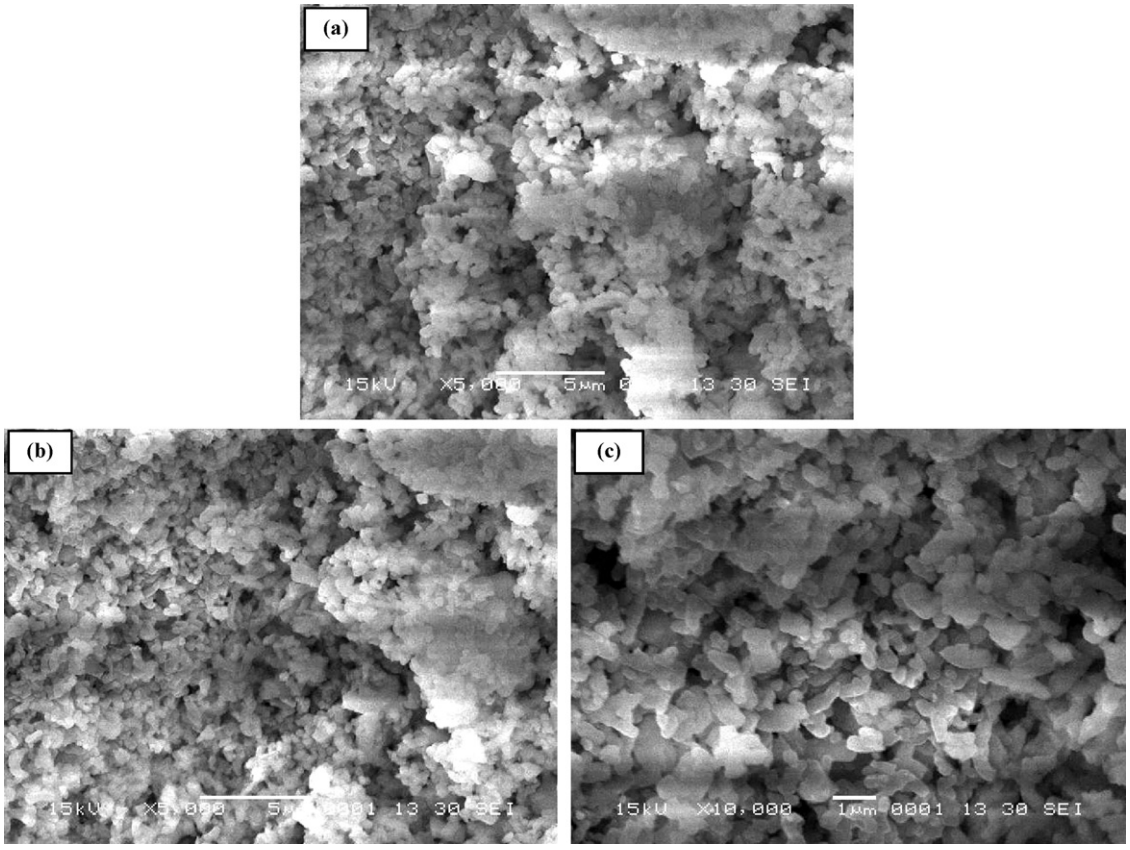

Fig. 6. SEM images of (a) Fe-MCM-41 (100), (b) Fe–Zn-MCM-41 (100) and (c) Zn-MCM-41 (100).

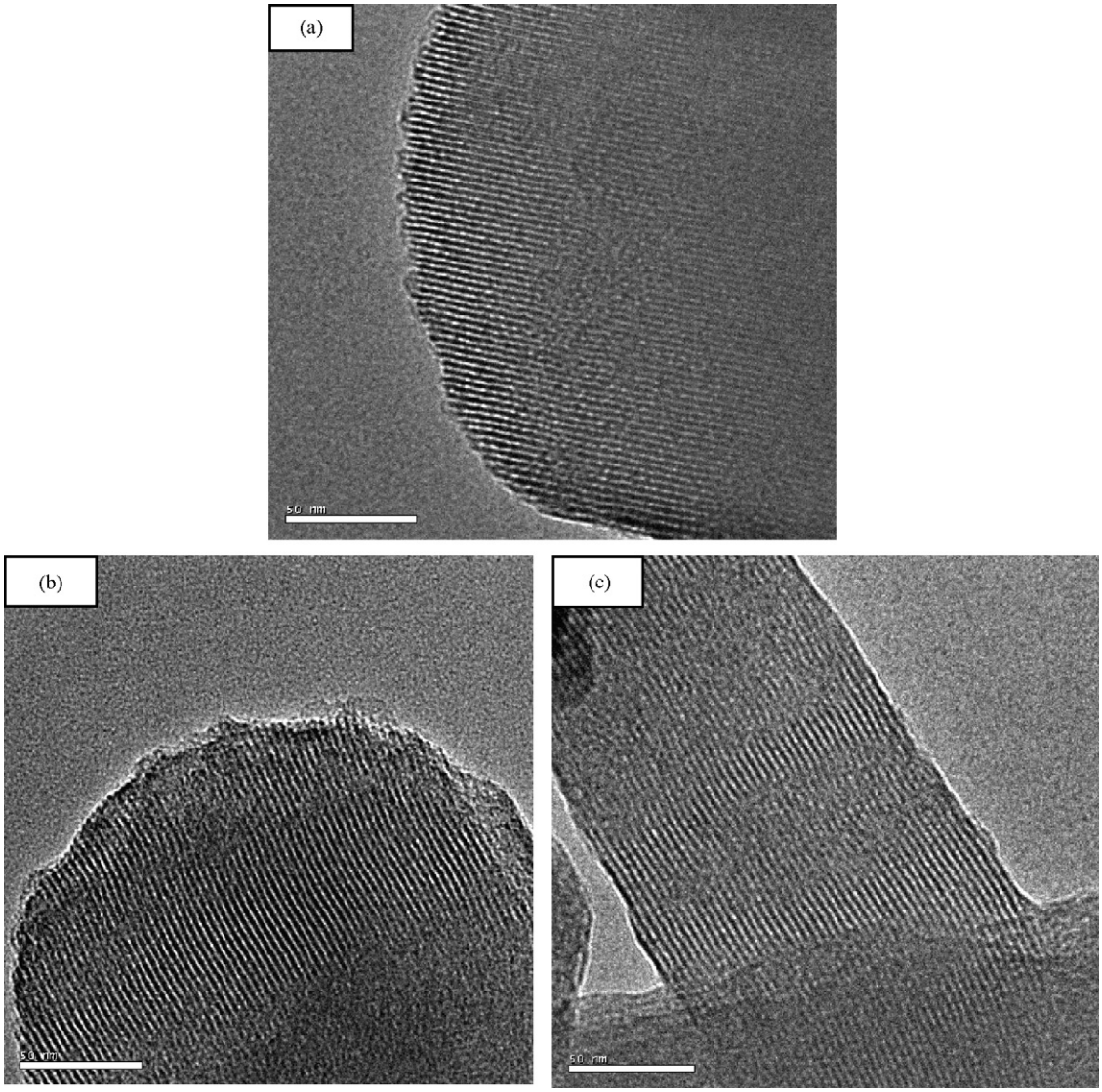

Fig. 7. TEM images of (a) Fe-MCM-41 (100), (b) Fe–Zn-MCM-41 (100) and (c) Zn-MCM-41 (100).

of the materials. TEM images indicate that the synthesized materials exhibit a well-ordered hexagonal array of regular pores as commonly known for MCM-41 materials [30].

3.2. Characterization of carbon nanotubes

3.2.1. Optimizing metal ratio for the high yield synthesis of CNTs

Fe and Zn are added in various ratios of 1:1, 1:2, 1:3, 1:4, 4:1, 3:1 and 2:1 on to the MCM-41 support. The ratio of Fe:Zn of 3:1 was found to be optimum for the formation of high yield of SWNTs rather than other ratios were shown in Table 2. This might be due to the 3:1 ratio of Fe:Zn, Zn ions are much more active and reduces the iron, which in turn is more responsible for the formation of SWNTs. Whereas in other ratios, Zn ions were not very active in the formation of carbon nanotubes. Moreover, Fe–Zn-MCM-41 with Fe:Zn (3:1) was found to show higher yield of SWNTs than Fe-MCM-41 and Zn-MCM-41.

3.2.2. SEM and TEM images of CNTs

The quality of the prepared nanotube material was characterized by TEM and SEM. The SEM image shows the morphology of CNTs, where a large number of carbon filament along with catalyst particles and amorphous carbon was found in the grown sample. Deposition of carbon filament over Fe–Zn-MCM-41 is more extensive than over Fe-MCM-41 or Zn-MCM-41, as observed from SEM (Fig. 8(a–c)). This was further supported by observations through TEM, the images of which are shown in Fig. 9(a and b). The image also clearly indicates the formation of carbon nanotubes over mesoporous Fe–Zn-MCM-41 materials. The diameter of the carbon nanotubes was found to be 2.1 nm by TEM.

Table 2
Formation of carbon nanotubes on synthesized mesoporous catalysts.

Catalyst (Si/M ratio)	Ratio of Fe:Zn	Deposition of carbon (%)
Fe-MCM-41 (100)	–	85
Fe–Zn-MCM-41 (100)	1:1	73
Fe–Zn-MCM-41 (100)	1:2	70
Fe–Zn-MCM-41 (100)	1:3	63
Fe–Zn-MCM-41 (100)	1:4	55
Fe–Zn-MCM-41 (100)	2:1	75
Fe–Zn-MCM-41 (100)	3:1	99
Fe–Zn-MCM-41 (100)	4:1	80
Zn-MCM-41 (100)	–	50

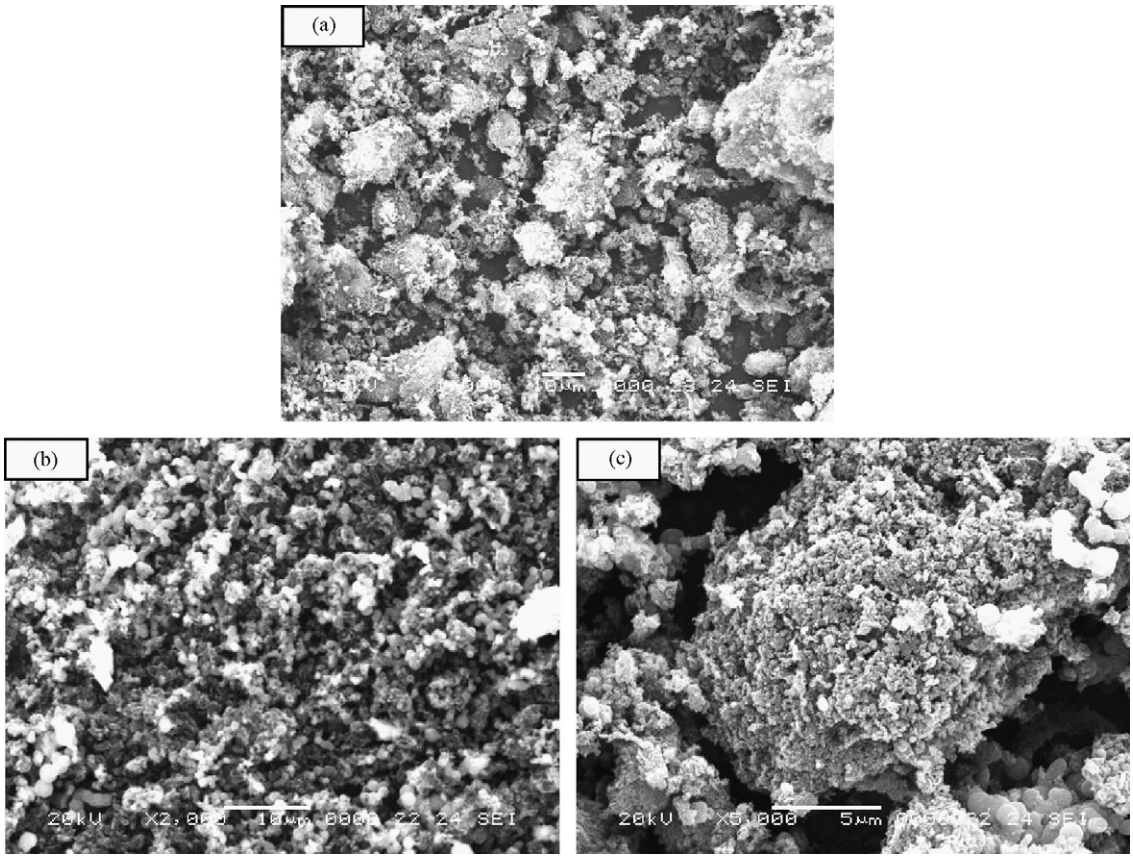

Fig. 8. SEM images of carbon nanotubes synthesized over (a) Fe-MCM-41 (100), (b) Fe–Zn-MCM-41 (100) and (c) Zn-MCM-41 (100).

3.2.3. Raman spectroscopy studies of CNTs

Raman spectroscopy is one of the most powerful tools for characterization of carbon nanotubes. All allotropic forms of carbons are active in Raman spectroscopy [31]. The forms are fullerenes, carbon nanotubes, amorphous carbon, polycrystalline carbon, etc. The position, width, and relative intensity of bands are modified according to the carbon forms [32]. The spectrum shown in Fig. 10 represents the formation of SWNTs formed over Fe–Zn-MCM-41 with Fe:Zn (3:1). The spectrum shows three distinct peaks corresponding to (i) a low-frequency peak at <300 cm^{-1} characteristic of the SWNT assigned to a A_{1g} "breathing" mode of the tubes, whose frequency depends essentially on the diameter of the tube (RBM, radial breathing mode); (ii) a peak at 1337.51 cm^{-1} assigned to residual ill-organized graphite, the so-called D-line (D, disorder); and (iii) a high-frequency (1590.92 cm^{-1}) called G band also characteristic of nanotubes, corresponding to a splitting of the E_{2g} stretching mode of graphite [33]. The radial breathing mode (RBM) usually occurring in the low-frequency region (100–350 cm^{-1}) is generally considered as a special signature of SWNT. There are several RBM peaks in the range of 100–300 cm^{-1} in Fig. 10 corre-

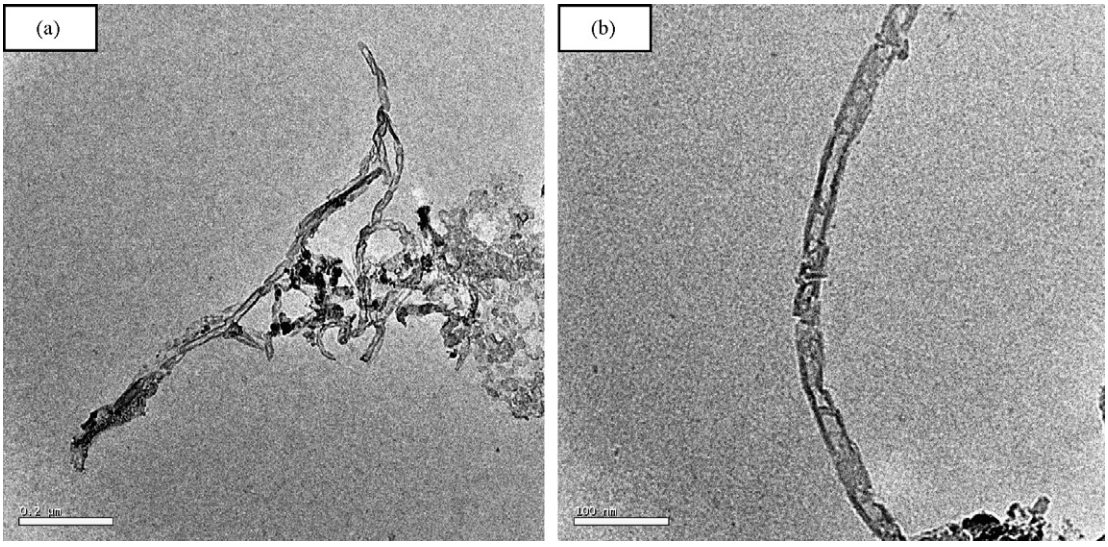

Fig. 9. TEM images of purified carbon nanotubes over Fe–Zn-MCM-41 catalyst.

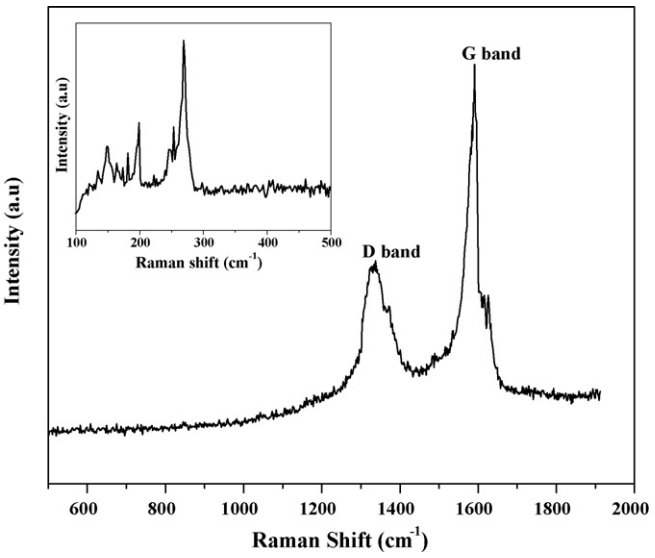

Fig. 10. Raman spectrum of CNTs over Fe–Zn-MCM-41 catalyst.

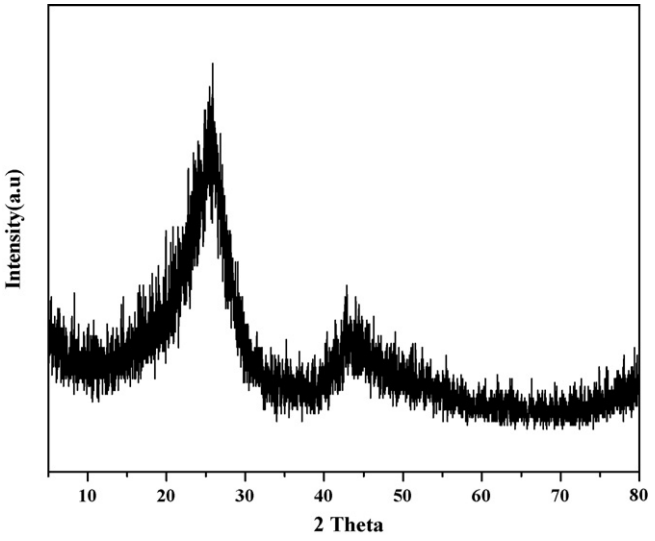

Fig. 11. XRD patterns of purified CNTs over Fe–Zn-MCM-41 catalyst.

sponding to SWNT diameters in the range of 1.2–2.5 nm on the basis of the following relationship, $d = 223.75/\lambda$ (where d = diameter and λ = wavelength) [34]. The intensity ratio of D to G band indicates well-graphitized CNTs.

3.2.4. X-ray diffraction pattern of CNTs

The XRD pattern of CNT is shown in Fig. 11. The pattern displayed a strong signal and weak signal at $2\theta = 25.6^\circ$ and 43.9°, which are assigned to (0 0 2) and (1 0 0) reflections of typical graphite, respectively. This result indicates that CNTs are well graphitized [35].

4. Conclusion

In the catalytic synthesis of carbon nanotubes over supported Fe–Zn-MCM-41 catalysts, the ratio of Fe:Zn of 3:1 was found to produce single-walled carbon nanotubes in large quantity. The synthesis yield was easily estimated, after removing the support by a simple acidic treatment to obtain a product containing SWNTs of high purity. This method of synthesis could replace the other two techniques of SWNTs production, because of the lower temperature used (700–900 °C), low cost of production and its industrial application potential. The formation of SWNTs with a diameter in the range of 1.5–2.5 nm is observed from a Raman spectrum. The good thermal stability and high productivity observed in this study suggested that the Fe–Zn-MCM-41 mesoporous molecular sieves could be a kind of promising supports for catalytically synthesizing SWNTs.

Acknowledgement

The authors would like to thank the Department of Science & Technology (SR/S5/NM-35/2005) under Nanoscience and Technology Initiative for providing financial support. One of the authors Mr. R. Atchudan is thankful to Council of Scientific and Industrial Research (CSIR), India, for providing Senior Research Fellowship.

References

[1] S. Iijima, Nature 354 (1991) 56.
[2] S. Iijima, T. Ichihashi, Nature 356 (1993) 737.
[3] M.M.J. Treacy, T.W. Ebbesen, J.M. Gibson, Nature 381 (1996) 678.
[4] Y. Nakayama, S. Akita, Y. Shimada, Jpn. J. Appl. Phys. 34 (1995) L10.
[5] A.C. Dillon, K.M. Jones, T.A. Bekkedahl, C.H. Kiang, D.S. Bethune, M.J. Haben, Nature 86 (1997) 377.
[6] D.S. Bethune, C.H. Kiang, M.S. deVries, G. Gorman, R. Savoy, J. Vazquez, R. Beyers, Nature 363 (1993) 605.
[7] T. Guo, P. Nikolaev, A. Then, D.T. Colbert, R.E. Smalley, Chem. Phys. Lett. 243 (1995) 49.
[8] V. Ivanov, J.B. Nagy, P. Lambin, A. Lucas, Chem. Phys. Lett. 223 (1994) 329.
[9] H. Ago, S. Imamura, T. Okazaki, T. Saito, M. Yumura, M. Tsuji, J. Phys. Chem. B 109 (2005) 10035.
[10] K. Hata, D.N. Futaba, K. Mizuno, T. Namai, M. Yumura, S. Iijima, Science 306 (2004) 1362.
[11] S.C. Lyu, B.C. Liu, S.H. Lee, C.Y. Park, H.K. Kang, C.W. Yang, C.J. Lee, J. Phys. Chem. B 108 (2004) 1613.
[12] P.B. Amama, S. Lim, D. Ciupura, Y. Yang, L. Pfefferle, G.L. Haller, J. Phys. Chem. B 109 (2005) 2645.
[13] B.C. Liu, S.C. Lyu, S.I. Jung, H.K. Kang, C.W. Yang, J.W. Park, C.Y. Park, C.J. Lee, Chem. Phys. Lett. 383 (2004) 104.
[14] R.G. Lacerda, A.S. The, M.H. Yang, K.B.K. Teo, N.L. Rupesinghe, S.H. Dalal, K.K.K. Koziol, D. Roy, G.A.J. Amaratunga, W.I. Milne, M. Chhowalla, D.G. Hasko, F. Wyczisk, P. Legagneux, Appl. Phys. Lett. 84 (2004) 269.
[15] C.N.R. Rao, B.C. Satishkumar, A. Govindaraj, M. Nath, ChemPhysChem 2 (2001) 78.
[16] C.T. Kresge, M.E. Leonowicz, W.J. Roth, J.C. Vartuli, J.S. Beck, Nature 359 (1992) 710.
[17] J.S. Beck, J.C. Vartuli, W.J. Roth, M.E. Leonowicz, C.T. Kresge, K.D. Schmitt, C.T.W. Chu, D.H. Olson, E.W. Sheppard, S.B. McCullen, J.B. Higgins, J.L. Schlenker, J. Am. Chem. Soc. 114 (1992) 10834.
[18] A. Corma, Chem. Rev. 97 (1997) 2373.
[19] Y. Chen, D. Ciuparu, S. Lim, G.L. Haller, L.D. Pfefferle, Carbon 44 (2006) 67.
[20] T. Somanathan, A. Pandurangan, Appl. Surf. Sci. 254 (2008) 5643.
[21] T. Somanathan, A. Pandurangan, Ind. Eng. Chem. Res. 45 (2006) 8926.
[22] Y. Li, W. Kim, Y. Zhang, M. Rolandi, D. Wang, H. Dai, J. Phys. Chem. B 105 (2001) 11424.
[23] B. Zheng, Y. Li, J. Liu, Appl. Phys. A 74 (2002) 345.
[24] M. Urban, D. Mehn, Z. Konya, I. Kiricsi, Chem. Phys. Lett. 359 (2002) 95.
[25] T. Suzuki, S. Inoue, Y. Ando, J. Mol. Catal. A: Chem. 17 (2008) 1596.
[26] A. Chen, Y. Lepage, A. Sayari, Chem. Mater. 7 (1995) 1015.
[27] S.J. Gregg, K.S.W. Sing, Adsorption Surface Area and Porosity, 2nd ed., Academic Press, New York, 1982.
[28] C.Y. Chen, H.X. Li, M.E. Davis, Micropor. Mater. 2 (1993) 17.
[29] S. Subramanian, A. Mitra, C.V.V. Satyanarayana, D.K. Chakrabarty, Appl. Catal. A 159 (1997) 229.
[30] S. Lim, D. Ciuparu, Y. Yang, G. Du, L.D. Pfefferle, G.L. Haller, Micropor. Mesopor. Mater. 101 (2007) 200.
[31] S. Arepalli, P. Nikolaev, O. Gorelik, V. Hadjiev, W. Holmes, B. Files, L. Yowell, Carbon 42 (2004) 1783.
[32] A. Ferrari, J. Robertson, Phys. Rev. B 61 (2000) 14095.
[33] A.A. Mamedov, N.A. Kotov, M. Prato, D.M. Guldi, J.P. Wicksted, A. Hirsch, Nat. Mater. 1 (2002) 190.
[34] S. Bandow, S. Asaka, Y. Saito, A.M. Rao, L. Grigorian, E. Richter, P.C. Eklund, Phys. Rev. Lett. 80 (1998) 3779.
[35] J.C. Juan, Y. Jiang, X. Meng, W. Cao, M.A. Yarmo, J. Zhang, Mater. Res. Bull. 42 (2007) 1278.